

SURFACE EFFECT ON ELECTRONIC, MAGNETIC AND OPTICAL PROPERTIES OF PtCoBi HALF-HEUSLER: A DFT STUDY

The electronic, magnetic, and optical properties of PtCoBi half-Heusler compound [001] surfaces and its bulk state have been investigated in the framework of density functional theory using GGA approximation. The half-metallic behaviors of CoBi-term, CoPt-term and PtBi-term decrease with respect to its bulk state. The spin polarization at the Fermi level is 73.2% for the bulk state, and it is -64.4% and -64.1% for the CoBi-term and PtBi-term, respectively while less polarization has been observed for the CoPt-term. All terminations have given almost similar optical responses to light. Plasmon oscillations for the terminations occur in the range of 12.5 to 14.5 eV (21 to 22 eV) along xx (zz), and it occurs at 23 eV for the bulk state. The refractive index for the bulk and all three terminations is very high in the infrared and visible areas, meaning a very strong metallic trend in these compounds. The phenomenon of super-luminescence occurs for the incident light with energy exceeding 5.5 eV for all three terminations, and it occurs in the range of 10 eV for the bulk mode. These terminations show transparent behavior after the energy of 10 eV.

Keywords: PtCoBi; [001] film; DFT; Electronic property; Optical property

1. Introduction

In recent years, much attention has been paid to ferromagnetic half-metals to be used in the spintronics [1-7] and optoelectronics industries [8-14]. More over, other two-dimensional materials are used in the optoelectronics industries [15-19]. Ideal half-metals are a group of material having metallic behavior in the majority spin and the semiconductor properties in the minority one [20-22]. The most important half-metal structures are binary and Heusler compounds. The Heusler structures are crystallized based on zincblende structure and are divided into two classes; full-Heusler and half-Heusler. Half-Heusler compounds with the space group number 216 crystallize in three phases of α , β , and γ . In their unit cell, there are three atoms with XYZ stoichiometry, with the X, Y, and Z atoms at (0, 0, 0) and (1/4, 1/4, 1/4) and (1/2, 1/2, 1/2) for α , β and γ phases [23-28].

The relatively high Curie temperatures of the half-Heusler composites, their structural conformity with semiconductor substrates, and their interesting optical and electronic properties have made these semiconductors very attractive. Recently, the structural and electronic properties of PtXBi semiconductors (with X = Mn, Fe, Co, and Ni) have been computationally

considered, and the results show that PtCoBi is half metal in all three phases of α , β and γ [29].

In the spintronic and optoelectronic industries, thin films of semiconductor compounds are used, so their surface effects and their interface are the most important and challenging points. Much theoretical and experimental work has been recently done in this field, but as the Heusler structures are crystallized in the zincblende phase, the two types of films with [001] and [111] terminations are more likely to grow. The density functional theory (DFT) and FP-LAPW+lo method have been used to calculate the electronic, magnetic and optical properties of Co₂VAl graphene-like (GL) mono-layer by Boochani et al. [30]. While the GL state represents a strong half-metallic properties and 0.5 spin-flip gap as well as an integer magnetic moment (1.00), the grown films in (101) and (011) directions is calculated to exhibit metallic properties with low spin-polarization at the Fermi level. The CoFeHfGe compound has been investigated in (100) and (001) directions by Paudel et al. [31]. The half-metallicity is found to be destroyed due to the surface states. Additionally, the HfGe (100) direction has the highest spin polarization of 90.72%, thus, it has the potential applications in giant magneto-resistance devices. The spin-polarized first-principles method is employed

¹ ISLAMIC AZAD UNIVERSITY, DEPARTMENT OF PHYSICS, SCIENCE AND RESEARCH BRANCH, TEHRAN, IRAN

² ISLAMIC AZAD UNIVERSITY, DEPARTMENT OF PHYSICS, KERMANSHAH BRANCH, KERMANSHAH, IRAN

* Corresponding author: hanteh@srbiau.ac.ir



by Yang et al. [32] to investigate the half-metallicity and magnetic behaviors of different (001) surfaces of Y_2CrSn Heusler structure. Using the generalized gradient approximation (GGA) method, the spin polarizations that has been calculated for two various terminations of the standard stable YSn -terminated and the artificial stable $SnSn$ -terminated are -96.9% and -95.8% , respectively, while it is -69.2% and -83.0% , respectively, using the GGA+U method, indicating the potential applications in spintronic devices. Hussain et al. [33] claimed that the confirmed half-metallicity in the $YCoCrGe$ bulk structure is appeared to be failed in all investigated 2D structures except the Cr-termination, with spin polarization about 64% and 76% for Y-Ge and Cr-Co, respectively, and 70% , 51% , and 68% for the Y, Co, and Ge surfaces, respectively. Moreover, the half-metallicity is observed to be confirmed in the Cr-terminated surface with spin polarization equal to 100% . Spin-polarized first-principles calculations are performed by Yang et al. [34] to examine the structural, electronic and magnetic properties in bulk state and variety of (001) surfaces of X_2CoIn ($X = Ti, Zr$) Heusler alloy. The $InIn$ and XIn terminations are the most stable surface and the second stable one, respectively. Hence, the $InIn$ termination, as the most stable surface, has high spin polarizations of 80.8% and 69.6% for $X = Zr$, respectively, and 65.2% and 62.3% for $X = Ti$, respectively. For two quaternary Heusler compounds of $NbFeCrAl$ and $NbFeVGe$, the structural, electronic and magnetic properties in the bulk structure and (001) surfaces are studied by Y. Li et al. [35] in the density functional theory framework using first-principles calculations. The half-metallic behavior is devastated for the Fe-V, Fe-Cr, Nb-Ge, and Nb-Al terminations of the (001) surfaces, such that the spin polarization ratio experiences a dramatic decline to less than 50% for $NbFeCrAl$ and $NbFeVGe$ compounds. Therefore, in this study, the effects of [001] thin film surfaces on the electronic and optical behaviors are studied and compared for the first time for the $PtCoBi$ half-Heusler composition in the γ phase.

Section 2 provides the details of the calculations, and Section 3 compares the structural, magnetic, electronic and optical behaviors of the films.

2. Computational methods

The electronic and optical properties of the $PtCoBi$ half-Heusler and its [001] film terminations have been considered with Wien2K code [36] based on the density functional theory (DFT) by full-potential (linear) augmented plane waves plus local orbitals (FP-LAPW+lo) [37] and the exchange-correlation potential has been approximated by PBE-GGA [38]. The optimized input parameters such as Kpoints was selected 4000 for bulk and 500 for films, as well as Rkmax and Gmax to 8.5 and 13.5, respectively. The atomic forces on the film structures were optimized to 1.0 mRyd/a.u. by mini-position command and the self-consistent calculations are considered to be stopped when the charge convergence is less than 0.0001 e. Besides, the optical calculations were approximated by RPA method [39].

3. Results

3.1. Structural properties

The slabs of nine atomic layers of the $PtCoBi$ compound in the γ phase along [001] crystal direction have been created. The three terminations of CoBi-term, CoPt-term and PtBi-term were considered for this compound. On both sides of the slabs, a vacuum of 30 Bohr was added to eliminate interactions. Fig. 1 shows an overview of the bulk state and the three terminations mentioned above. To investigate state of the bulk and the terminations, which are stable in the two ferromagnetic and non-magnetic states, the total energy curve is plotted in terms of volume, fitted by the Murnaghan equation of state, for the bulk and all three terminations with the ratio of $c/a = \text{constant}$ in the two states: the ferromagnetic (FM) and non-magnetic (NM), which are plotted in Fig. 2. As it can be seen from the curves, the bulk and all three terminations of CoBi-term, CoPt-term, and PtBi-term are more stable in the ferromagnetic state than in the non-magnetic state because they are in lower energy than in the non-magnetic state. The transition pressure values of $PtCoBi$ compound and PtBi-term obtained 15.74 and 7.70 Gpa, respectively while there is no transition pressure for CoBi-term and CoPt-term.

3.2. Electronic Properties

The electronic structure of the material gives useful information about the physical behavior such as electronic, optical and transport properties. The electronic density of states is plotted in Fig. 3 for the $PtCoBi$ half-Heusler compound in the γ phase for the bulk state. It is clear that the electron density is anisotropic in the energy range from -2 eV to 1 eV, and the electronic behavior is different in both spins. The magnetic moment of $PtCoBi$ is obtained $1.381 \mu_B$ as reported in

Table 1 which is in a good agreement with the other works. Additionally, the spin polarization at the Fermi level is derived from the relationship $P = (N\uparrow - N\downarrow)/(N\uparrow + N\downarrow)$ which is 73.2% . There is not a necessity for the bulk material to be 100% spin polarized. There have been compounds where their spin polarization is less than 100% in the bulk state, but their spin polarization has remained constant or increased in the surface state [40,41]. It can be seen from Fig. 3 that the main cause of the magnetic anisotropy at the Fermi level belongs to the electronic states of Co atoms and, to some extent, Pt atoms. It can also be observed that the electronic states of the Bi atom at the Fermi level have a very small contribution compared to the other two atoms. Therefore, it can be concluded that this compound exhibits a dual behavior as the response to an applied external magnetic field. Most Heusler compounds in the industry are used in the form of thin films, so it is important to study the $PtCoBi$ composition behavior in the form of the thin film. In thin films, the surface effects cause changes in electron behavior, followed by changes in other behaviors such as optical and transport behaviors because

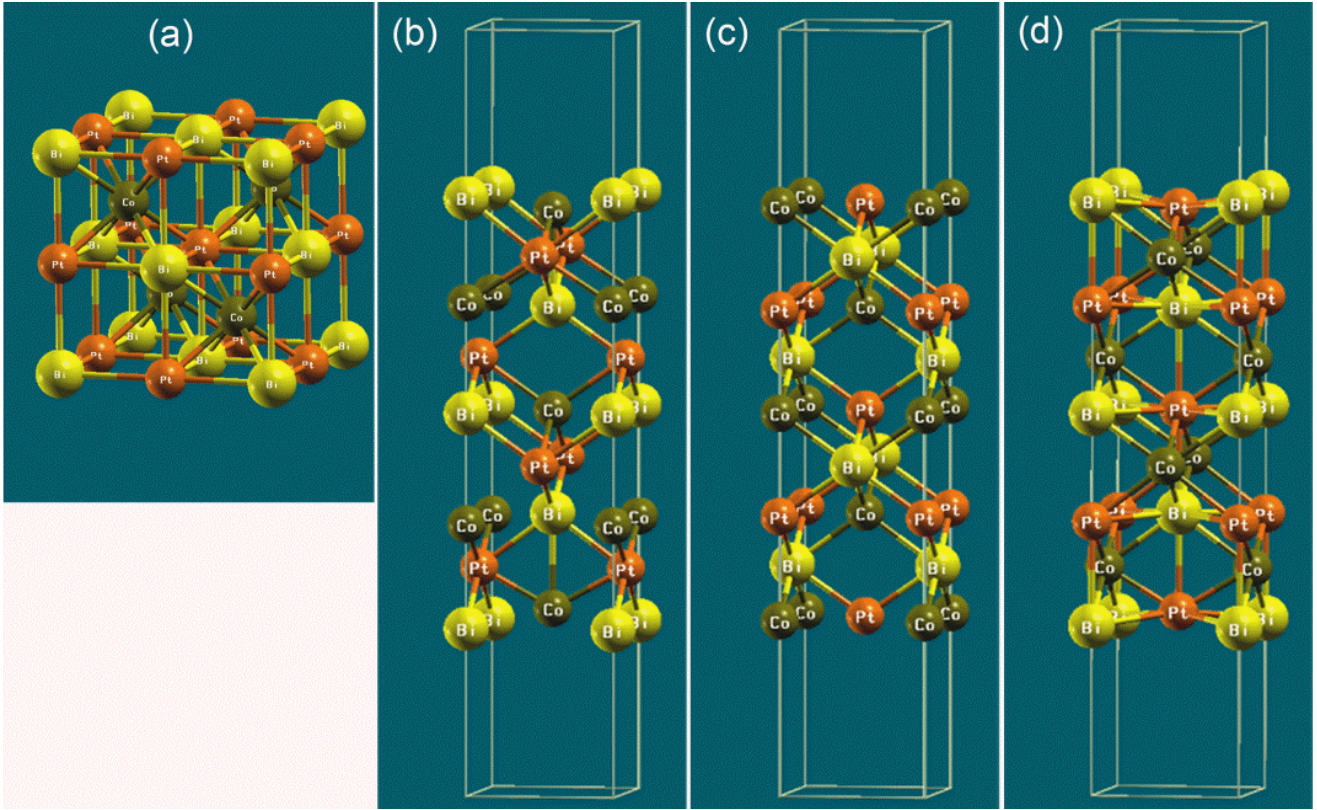


Fig. 1. The structures of (a) bulk (b) CoBi-term (c) CoPt-term and (d) PtBi-term

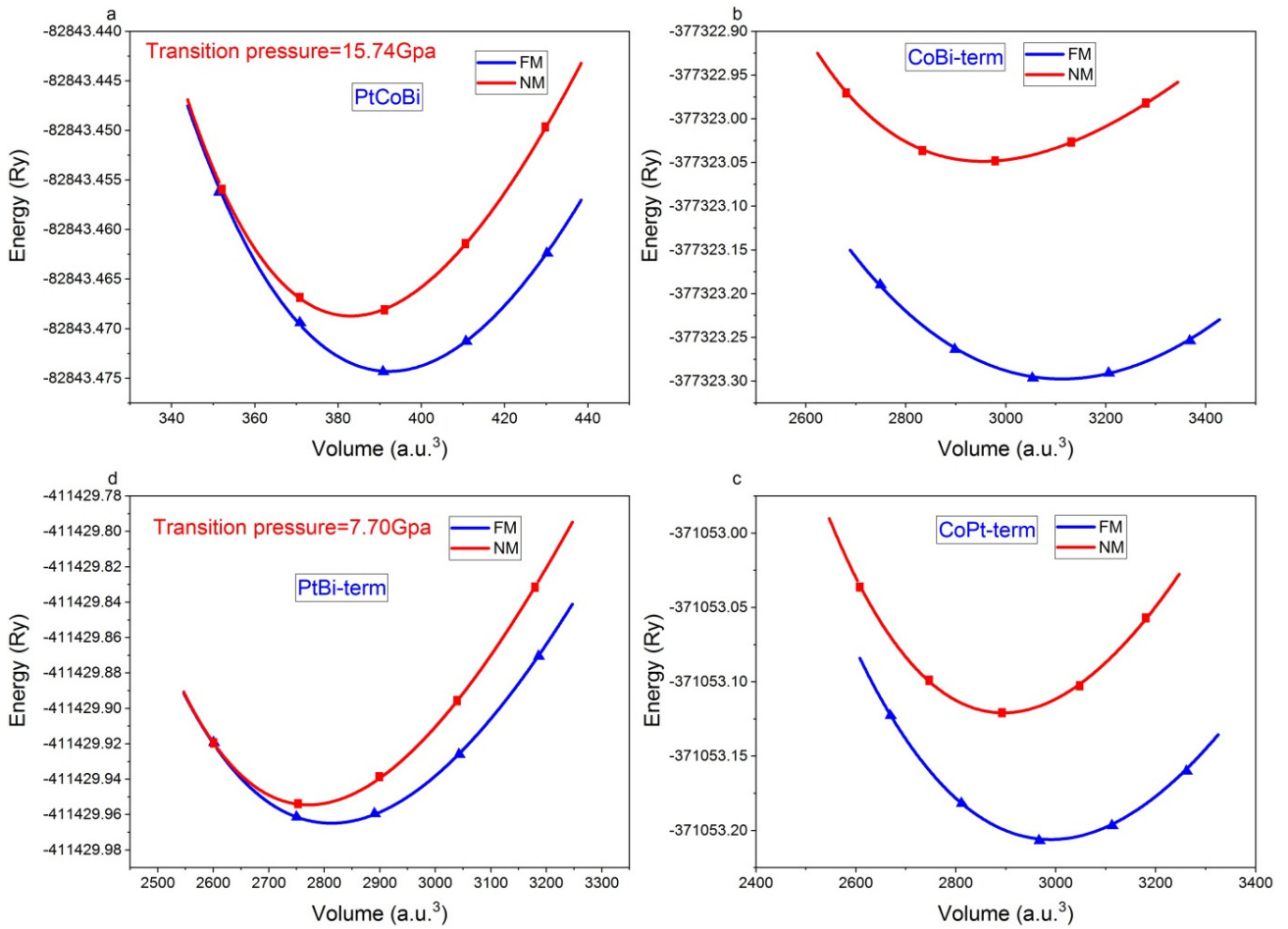


Fig. 2. The total energy in terms of a function of volume in the two states (FM) and (NM) for (a) bulk (b) CoBi-term (c) CoPt-term and (d) PtBi-term

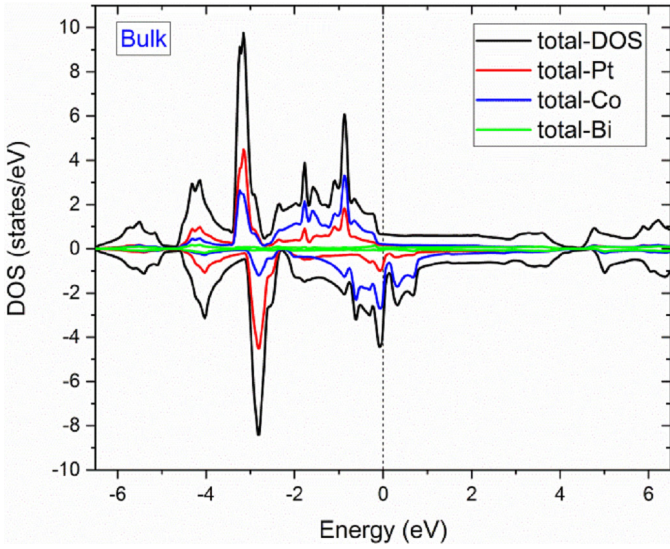


Fig. 3. The total and partial DOS of PtCoBi bulk in up and down (dn) spins

in thin-film structures, the increase in electron density at the surface and the presence of dangling bonds elevates the electrostatic potential at the film surface, with altering the physical nature of

the material. Due to the crystallization of PtCoBi structure based on the FCC structure, there are two important directions to grow the film: one is [001] and the other is [111].

Fig. 4 illustrates the electron density of states for the PtCoBi thin film in two spin channels with different terminations for [001] direction. The spin polarization values of all these films are listed in Table 1. Considering the DOS curves in Fig. 4, it is observed that at the terminations of CoBi-term and PtBi-term, the spin polarization is -64.4% and -64.1% , respectively, and at the termination of CoPt-term, less polarization is observed as the electron states in the spin-up are less than the spin-down ones.

Table 1 shows the total magnetic moment of PtCoBi half-Heusler compound and the CoBi-term, PtCo-term and PtBi-term, as well as the magnetic moment of the atoms forming the bulk and terminations from the first layer (the surface layer) to the fifth layer (the central layer). As it can be seen in Table 1, the magnetic moment of the surface atoms at each of three mentioned terminations has a significant increase or decrease due to the surface effects compared to the magnetic moment of similar atoms in the bulk state, with the largest increase (decrease) in the magnetic moment for the Co atom, which is equal to 52% (-36%) for CoBi-term (CoPt-term). This situation

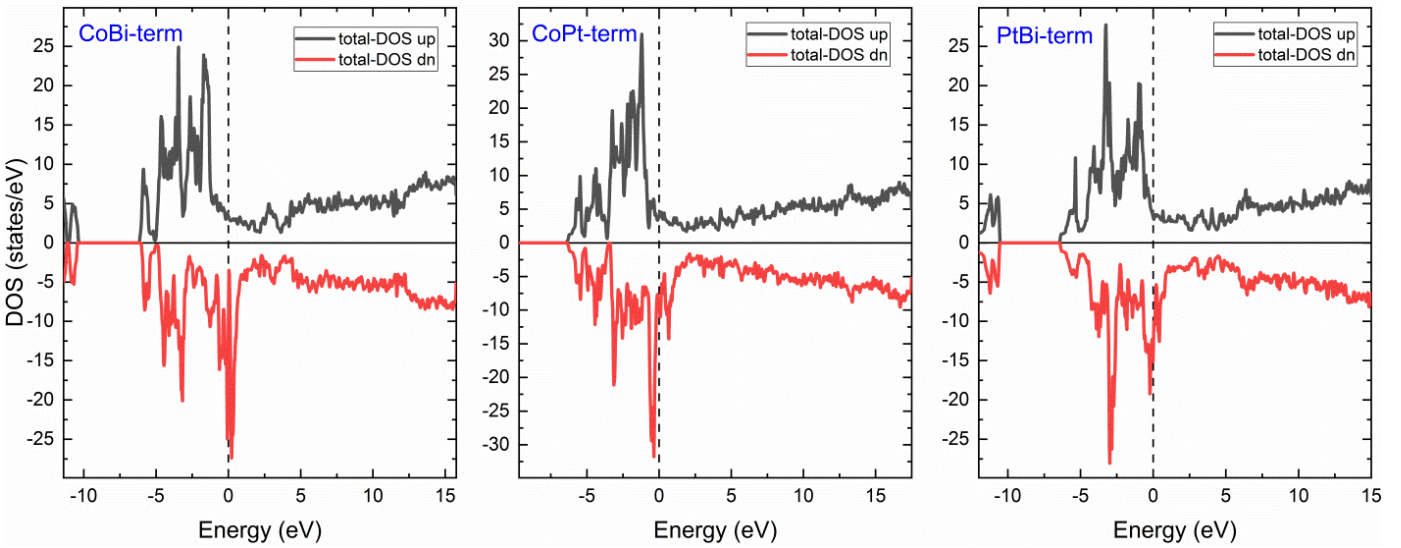


Fig. 4. The total DOS of CoBi-, CoPt- and PtBi terminations in up and down spins

TABLE 1

The spin polarization, total magnetic moment, and the magnetic moment of the atoms for all layers in all mentioned terminations

Magnetic Moment of terminations in μ_B						
Layer	Co-Bi-term		Co-Pt-term		Pt-Bi-term	
L ₁ (surface)	M(Co ₂) = 1.930	M(Bi ₁) = -0.021	M(Co ₂) = 0.808	M(Pt ₁) = 0.047	M(Pt ₂) = 0.124	M(Bi ₁) = -0.013
L ₂	M(Pt ₁) = 0.212		M(Bi ₁) = -0.023		M(Co ₁) = 1.361	
L ₃	M(Co ₁) = 1.837	M(Bi ₃) = 0.006	M(Co ₁) = 1.920	M(Pt ₃) = 0.024	M(Pt ₁) = 0.133	M(Bi ₃) = -0.005
L ₄	M(Pt ₂) = 0.184		M(Bi ₂) = -0.028		M(Co ₂) = 1.223	
L ₅ (central layer)	M(Co ₃) = 1.855	M(Bi ₂) = 0.006	M(Co ₃) = 1.219	M(Pt ₂) = 0.072	M(Pt ₃) = 0.177	M(Bi ₂) = -0.008
MMT	10.340		7.034		5.693	
Spin polarization	-64.4%		-40.7%		-64.1%	
Magnetic Moment of bulk in μ_B						
MMT = 1.381(1.443 Ref [22])	M(Pt) = 0.146		M(Co) = 1.269		P(Bi) = -0.008	

for magnetic moment shows only decrease for the Pt atom and just increase for the Bi atom so that the highest decrease for the Pt atom is -68% for CoPt-term and the highest increase for Bi atom is 162% for the CoBi-term. It seems that a decrease in the number of neighbors at the surface is the dominant factor in determining the magnetic moment. The magnetic moment of Co in the second (subsurface layer) and the third layers in the considered terminations have been increased in comparison with the bulk state, but the magnetic moment of Pt and Bi has fluctuated around the bulk value. In the central layer (fifth layer) of the terminations, the magnetic moment of the atoms tend to move toward the magnetic moment of similar atoms in the bulk due to the reduction of surface effects, so that the magnetic moments of the Co atom at CoPt-term and the Bi atom at PtBi-term are only slightly different.

In Fig. 5, the electrostatic potential curve along the crystal growth [001] is plotted for all three terminations of CoBi-term, CoPt-term, and PtBi-term. It can be seen that in all three films, Blach's behavior is detected along the z-axis, and at the film surface, there is a sharp escalation in the electrostatic potential. This increase is a factor to change the nature of electronics and electron transport in films. Fig. 5 indicates that the electrostatic potential in the PtBi-term film has the highest oscillation and the lowest oscillation occurs in the CoPt-term. Thus, the electron transport factor and magnetism in the PtBi-term termination are expected to have the high value.

In Fig. 6, the electron density curves are plotted for the surfaces of the terminations of the [001] films. It is obvious that in the spin-up for the CoPt-term termination, the highest electron density is at the position of the Co atoms, and by comparing the

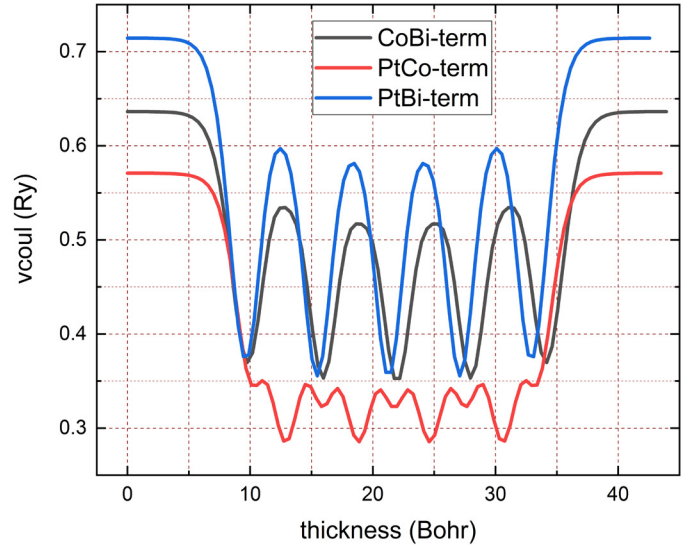


Fig. 5. The electrostatic potential of the CoBi-, CoPt- and PtBi-terminations along [001] direction

graphs at the two spins up and down, it is clear that the electron density gradient in the spin-down has changed significantly as the bonds in the spin-down become more ionic. In the CoBi-term termination, the form of electron density changes differs in both spins, as a dipole appears at the location of the Co atom at the film surface, and the electron density distribution has not changed much at the Bi atom location. However, in the PtBi-term termination, the ratio of electron density changes from spin up to down belongs to the Bi atoms, and the electron density shape at the Pt atom location does not display much change. It can be

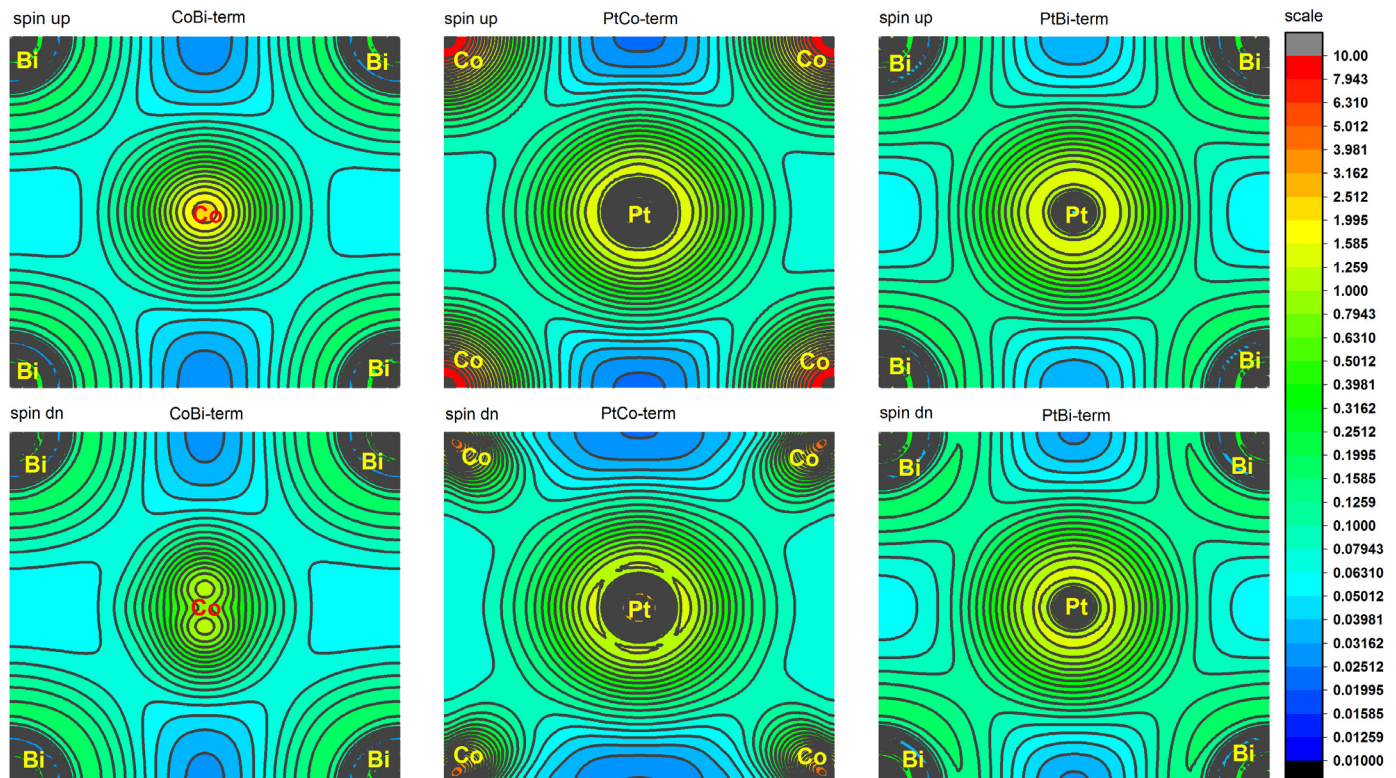


Fig. 6. The electron density of the film surfaces for two up and down spins

seen from the electron density, comparing the atoms in the up and down spins, the Pt-Bi bond at the Pt-Bi-term is stronger at the Co-Bi-term due to the greater electron density than the other two bonds at the other two terminations e.g. the Co-Pt bond at the Co-Pt-term and Co-Bi bond at the Co-Bi-term.

Comparing the bond length between the atoms located on the surface can be a suitable tool to study the interactions between the atoms on the surface. The length of Pt-Bi bond at the Pt-Bi-term is 3.157\AA , the length of Co-Pt bond at the Co-Pt-term is 3.087\AA and the length of Co-Bi bond at the Co-Bi-term is 3.061\AA . Shorter Pt-Bi bond length at the Pt-Bi-term is another reason why the bond is stronger than the two Co-Pt and Co-Bi bonds for the Co-Pt-term and Co-Bi-term terminations, respectively.

3.3. Optical Properties in the Bulk State

Fig. 7(a) represents the gamma phase absorption graph of the PtCoBi structure. As it is expected from the metallic nature of this compound, light absorption at the low energies (infrared region) starts with a steep slope, increases to 5 eV, and after several fluctuations rises to 18 eV. It then declined again with a sharp slope. This spectrum shows that based on the metallic behavior of the PtCoBi compound, the light absorption is continuous and it exists at all energy ranges up to 25 eV. Absorp-

tion can be due to a variety of reasons, including the transfer of electrons from lower levels to higher ones, or the acceleration of electrons inside the compound.

Fig. 7(b) shows the energy loss function (Eloss) spectrum so that there is the least energy loss at low energies, at the infrared, visible, and UV edge areas. Therefore, it demonstrates that the PtCoBi combination is a useful combination for use in infrared, visible and UV edge sensors, and the Eloss peak, which occurred at 23 eV, could be due to Plasmon oscillations. The extinction coefficient is one of the important physical parameters providing the amount of light penetrating the material. Fig. 7(c) represents that the PtCoBi has the highest extinction coefficient at lower energies (infrared and visible range), but there is a dramatic decline in the amount of light entering the thin film at the UV edge and higher energies as the extinction coefficient is virtually zero at 25 eV thereafter. It can be seen from the Fig. 7(a) that the light absorption is also very low, so at high energies, virtually all light passes through the object. Hence, PtCoBi actually acts as a transparent object, but by comparing the extinction coefficient and the Eloss, the composition can be said to be more useful for applications in the energy range of the UV edge.

The response of each object to the incident light is shown by the dielectric function, $\epsilon(\omega)$, which is a complex mathematical tensor. Fig. 7(d) provides the real part of the dielectric function, $\text{Re } \epsilon(\omega)$. At low energies, $\text{Re } \epsilon(\omega)$ has tended to $-\infty$, indicating its strong metal nature. Interestingly, it does not have any positive

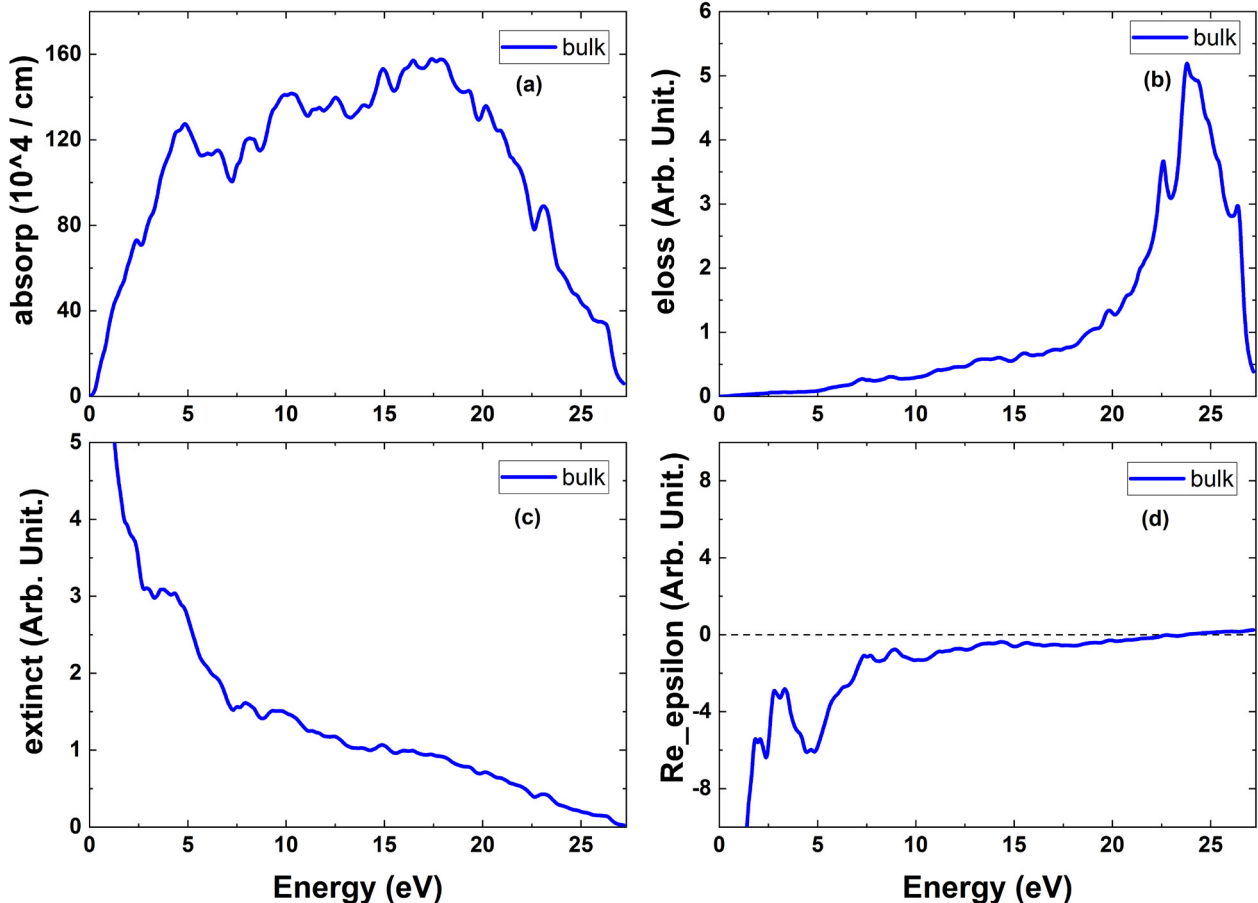


Fig. 7. (a) Absorption, (b) Eloss, (c) Extinction and (d) real part of dielectric function for PtCoBi bulk

response to the light at all energy ranges, especially the energy range of 0 to 7 eV. Nevertheless, it has a root at the energy of 23 eV, and it has transitioned from the negative area to the positive one at this point. This root is where Eloss also had a peak, so the Plasmon oscillations of this compound occur at the energy of 23 eV.

The imaginary part of the dielectric function, $\text{Im } \varepsilon(\omega)$, represents the electron transition from filled levels to the empty ones, and each peak corresponds to this electron transition. In Fig. 8(a), as it is expected from the metallic nature of the PtCoBi thin film, the major $\text{Re } \varepsilon(\omega)$ peaks occurred in the infrared and visible regions, decreasing with increasing photon energy delivered with a steep slope. Practically, no significant transition occurs after 10 eV. As mentioned above, after 25 eV, according to this fact that the absorption, $\text{Re } \varepsilon(\omega)$, the extinction coefficient and Eloss are zero, this compound is transparent.

The PtCoBi optical conductivity diagram in Fig. 8(b) shows that this compound has a very high optical conductivity at low energies. Additionally, it was mentioned that $\text{Im } \varepsilon(\omega)$ had a high electron transition in the infrared region indicating that all absorbed light is used for conduction. In Fig. 8(b), from the edge of the visible light to about 15 eV, optical conductivity has some fluctuations with a slight decrease in mean value. After 25 eV, the conductivity is zero, which is another evidence for the transparency of this compound. The high refractive index in Fig. 8(c) shows the metallic behavior for PtCoBi while it de-

creases with steep slope by increasing photon energy. After the UV edge, the refractive index magnitude becomes lower than one, demonstrating that the phase velocity of the electromagnetic spectrum in the object is greater than the speed of light in the vacuum. By further reducing the refractive index at higher energies, the transparency of this compound is again confirmed at energies above 25 eV.

The PtCoBi reflection coefficient in Fig. 8(d) is approximately 100% at low energies, indicating a very strong metallic nature in the infrared region, but the reflection coefficient decreases further in the visible region with more absorption and reduction of $\text{Im } \varepsilon(\omega)$ peaks. Consequently, it leads to a decline in its metallic behavior so that it exhibits semiconductor or even insulator behavior at energies above 25 eV resulting in a transparent behavior.

3.4. Optical Properties of Thin Film

Surface effects on thin films lead to fundamental changes in the physical behavior of materials. In this section, the optical properties are studied for the (001) PtCoBi films at the CoBi-term, CoPt-term, and PtBi-term terminations. The real parts of the dielectric functions, $\text{Re } \varepsilon(\omega)$, of these terminations are shown for both directions of xx and zz in Fig. 9(a) and 9(b). Given that in the (001) film, the crystal symmetry is broken compared to the

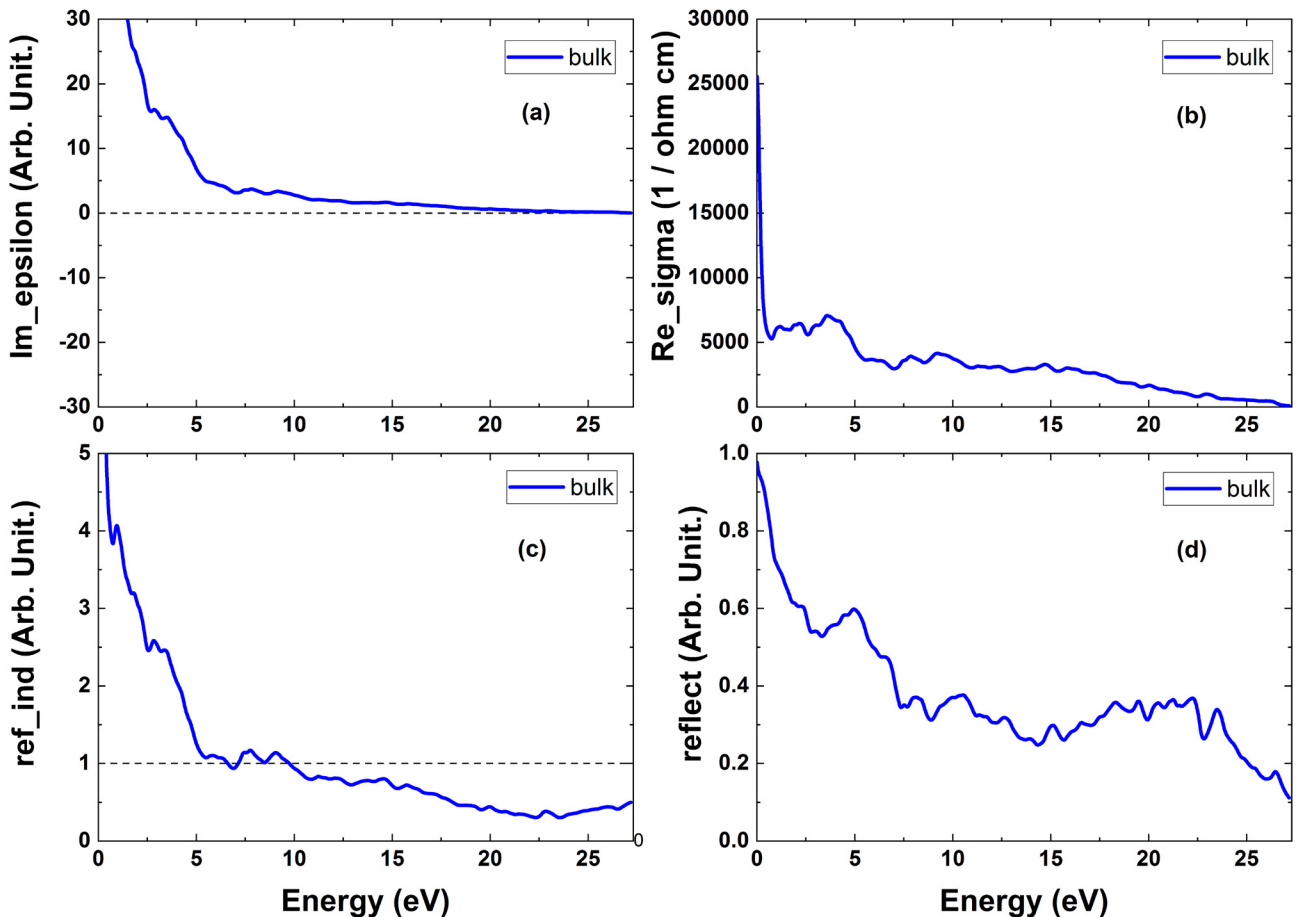


Fig. 8. (a) imaginary part of dielectric function, (b) real part of electric conductivity, (c) refraction index and (d) reflection index of the PtCoBi bulk

bulk state, optical response of the films, when the light electric field direction is parallel to the cross-sectional area of the film (xx axis), is accordingly expected to be different from when the light electric field direction along the crystal growth direction (zz axis). As it can be expected from the features of these films, these terminations exhibit very strong metallic behavior such that their static values of the real part of the dielectric function values in the xx and zz directions are $-\infty$ and $+\infty$, respectively. By com-

paring the optical spectra along both directions of xx and zz , it can be observed that the response of these films to the incident light differs in the infrared, visible and UV regions, so different optical responses can be obtained by changing the incident light. For the diagram of the real part of the dielectric function along xx direction, $\text{Re } \varepsilon(\omega)_{xx}$, it is clear that at the CoBi-term termination, the value of this parameter shifts from negative to zero, and it has a root in the visible region. Furthermore, there

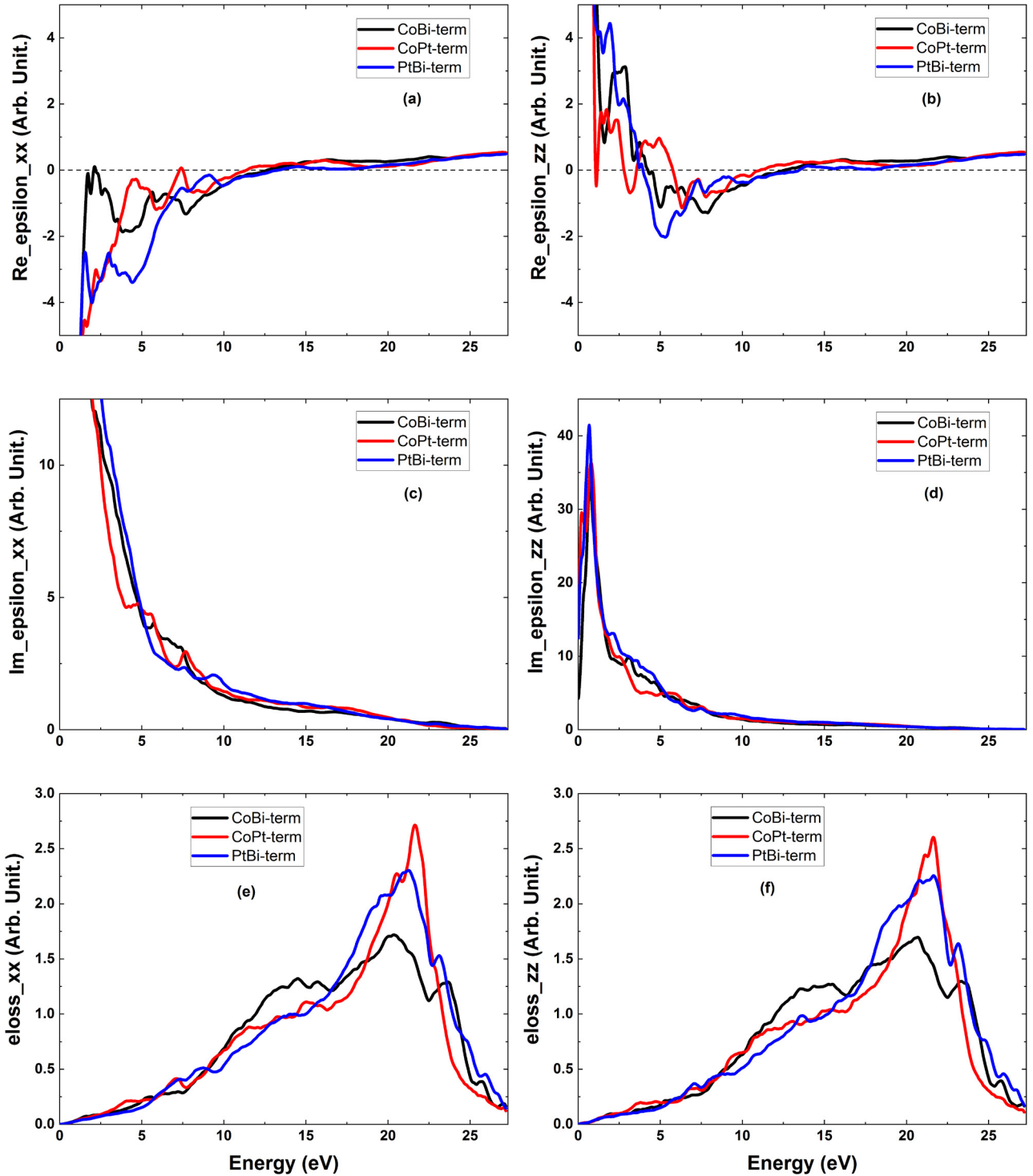


Fig. 9. (a) real part of dielectric function along x direction, (b) real part of dielectric function along z direction, (c) imaginary part of dielectric function along x direction, (d) imaginary part of dielectric function along z direction, (e) energy loss function (Eloss) along x direction, (f) energy loss function (Eloss) along z direction for the CoBi-, CoPt- and PtBi-termination

are two other negative peaks in the range of 4.5 to 7.5 eV. At the CoPt-term termination, $\text{Re } \varepsilon(\omega)_{xx}$ again approaches zero, one at 5.5 eV and the other at 7.5 eV beside a negative peak at 7 eV. It is obvious from the comparison of these two terminations that the CoBi-term termination experiences a redshift compared to the CoPt-term one, but the PtBi-term has more metallic behavior than the other two terminations because $\text{Re } \varepsilon(\omega)$ is negative in the infrared, visible and UV edge energy ranges, and its absolute magnitude is greater than the other two ones. The common point among all three terminations is that they have roots in the range of 12.5 to 13.5 eV. On the contrary, the real part of the dielectric function along zz , $\text{Re } \varepsilon(\omega)_{zz}$, has shown different behavior with positive responses to the incident light in the visible region. The highest response belongs to the PtBi-term termination, but in the UV edge range, the two terminations of PtBi-term and CoBi-term enter the negative area and have root. In the CoPt-term termination, an oscillatory behavior is observed in the range of 4 to 5 eV, and there are two roots. In the range of 4.5 to 12.5 eV, the real part of the dielectric function along zz is negative in all terminations. This means that in these regions, the electromagnetic waves do not propagate in these compounds and the absorptions and dissipations occur. Similarly [42], same as the xx direction, there is a root at 5 eV for the real part of the dielectric function along zz in the range of 12.5 to 13.5 eV.

In Fig. 9(c) and 9(d), the imaginary part of the dielectric function, $\text{Im } \varepsilon(\omega)$, in the xx and zz directions have been shown. Each peak of the imaginary part of the dielectric function represents an electron transition from a filled level to an empty one. It can be seen from the comparison of the imaginary part of the dielectric function in both the xx and zz directions that the static values of all three terminations in the xx direction tend to $+\infty$ while they start from zero in the zz direction and reach to the large peak with a steep slope in the infrared region. It can be concluded from this diagram that the metallic properties of the terminations are severely strong in the xx direction although it decreases along the zz direction. For the all terminations, the imaginary part values of the dielectric function drop with a dramatic slope for both xx and zz . Hence, it is observed that the electron transitions, which are due to the strong metallic behavior at the terminations, especially in the xx direction, occur in the infrared and visible areas, and they have reached a saturation level such that there is practically no significant transition at energies above 15 eV. As a result, the absorbed light is not consumed for the transition. In the zz direction, one thing to note is that except for a very sharp peak at the visible edge, no significant peak can be seen at other energies meaning that there is an optical instability in the behavior of these films along the zz direction.

Fig. 9(e) and 9(f) show the energy loss function (Eloss) which its peaks can represent Plasmon oscillations provided

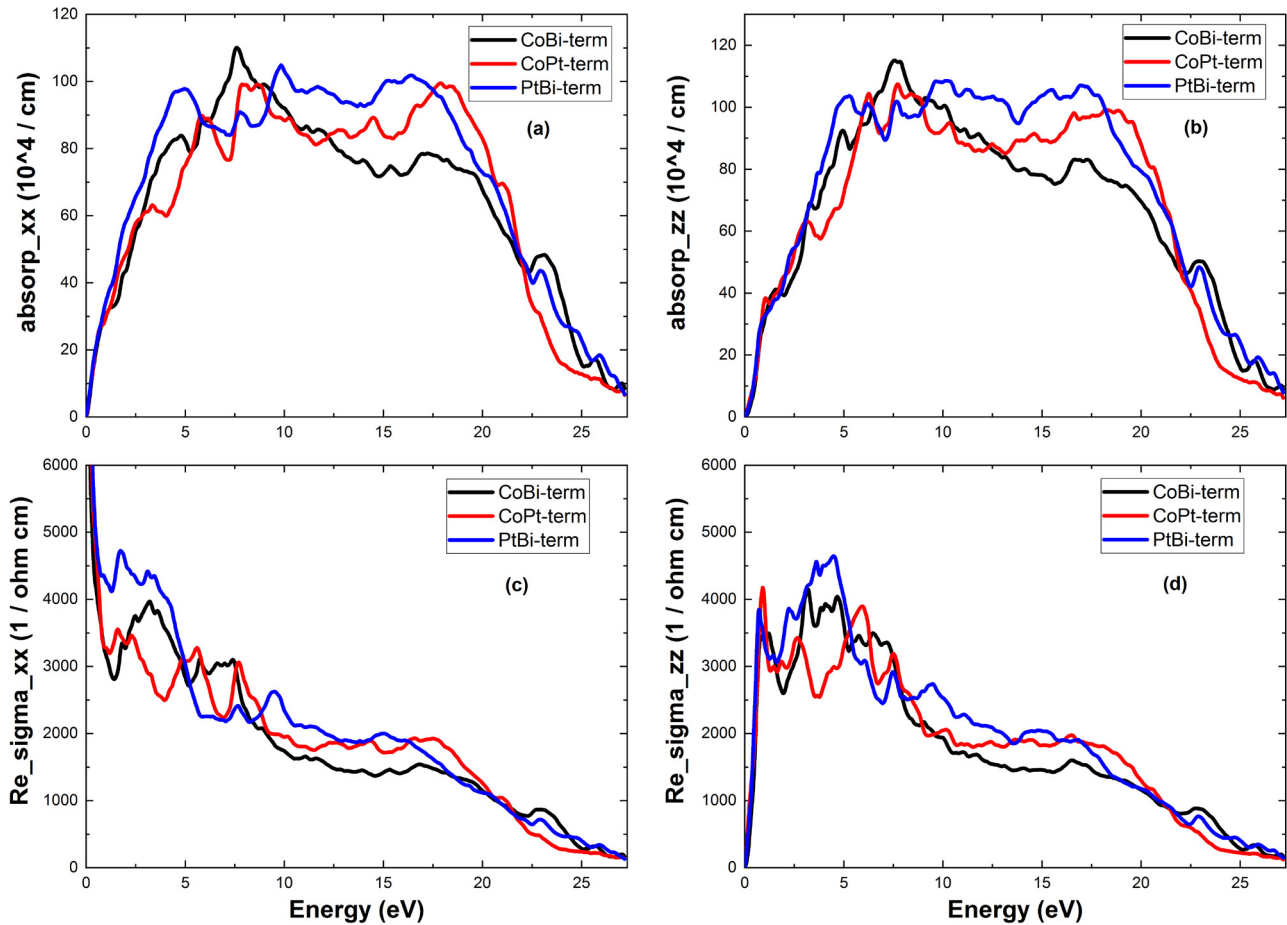


Fig. 10. (a) Absorption coefficients along x direction, (b) Absorption coefficients along z direction, (c) Conductivity along x direction and (d) Conductivity along z direction of the CoBi-, CoPt- and PtBi-terminations

that the real part of the dielectric function simultaneously has a root at the same energy. It is obvious in these figures that the Eloss has magnitude and peak in the two areas of 21 to 22 eV and 12.5 to 14.5 eV, respectively. Comparing with the real part of the dielectric function in these two directions, it is clear that there are Plasmon oscillations at these two points. The remarkable point is that the Eloss values in both directions are very small in the range of 0 to 5 eV, so the incident light is losing a very small amount of energy due to the high absorption in this area

as well as the high response of these terminations, which can be seen in Fig. 10(a) and 10(b). In Fig. 10(c) and 10(d), according to the extremely high optical conductivity of the terminations in the range of 0 to 5 eV, it can be concluded that these films are excellent optical transporter for electrons, but as the amount of Eloss increases, the optical conductivity decreases.

In Fig. 11(a) and 11(b), the refractive index diagram is plotted in the two directions. Clearly, the refractive index of all three terminations is very high for both directions in the

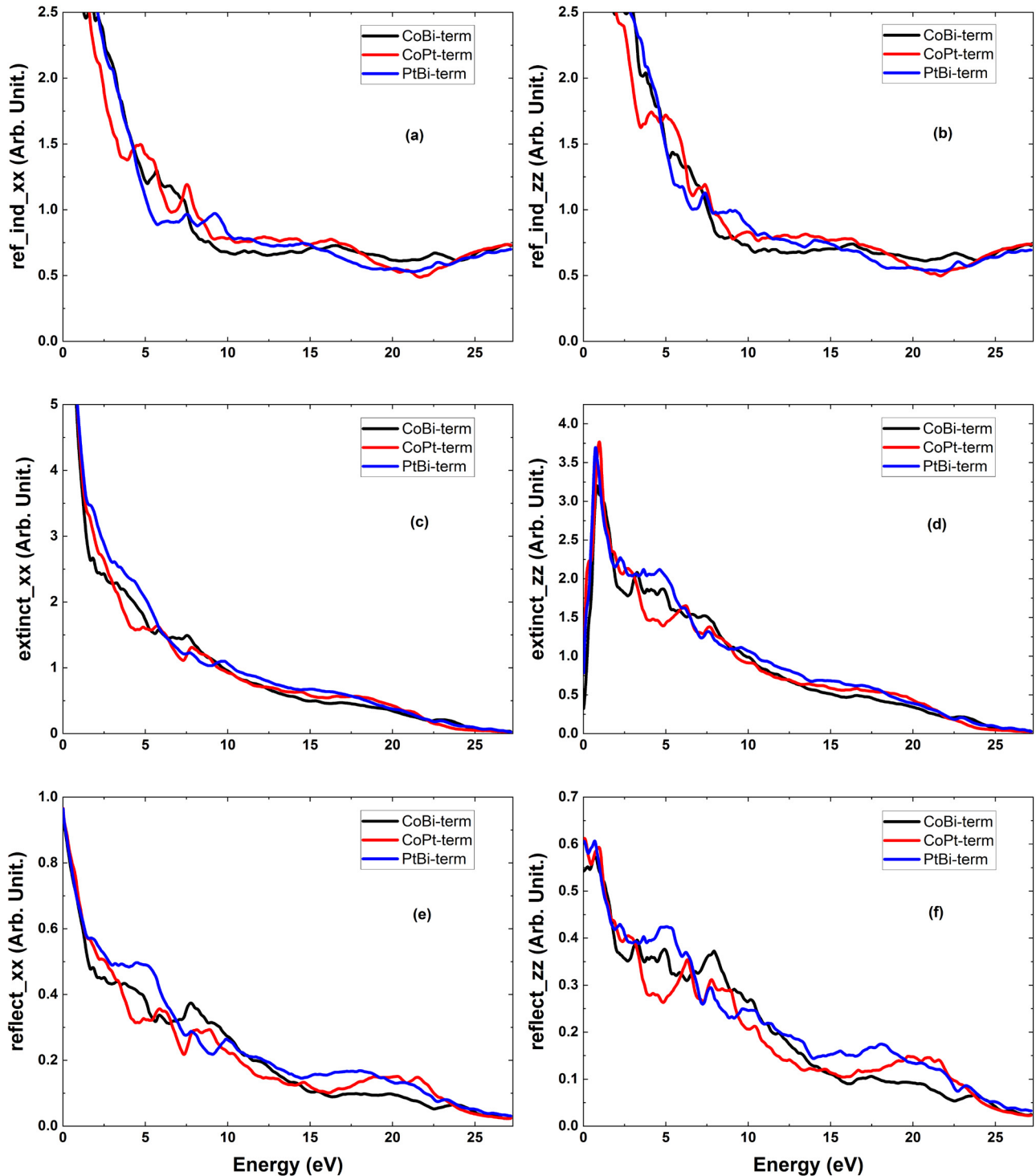


Fig. 11. (a, b) The refraction indexes along the x and z directions, (c, d) Extinction coefficients along with the x and z directions and (e, f) Reflections along with the mentioned directions for CoBi-, CoPt- and PtBi-terminations

REFERENCES

infrared and visible regions and tends to $+\infty$ meaning a very strong metallic property in these compounds. After the range of 5.5 eV, the refractive index values are lower than unity, and they exhibit milder behavior with a gentle slope, indicating a super-luminance phenomenon. The refractive index values are lower than unity mean that the phase velocity ($v = c/n$) of the electromagnetic spectrum is greater than light velocity in a vacuum, c [43,44].

The extinction coefficient represents the light permeability in the material, and their peaks determine the rate of decrease in the incident light amplitude. In Fig. 11(c), for all three terminations, all static values of the extinction coefficients of these combinations in the xx direction tend to ∞ , so in the infrared, visible, and UV edge area, there are the most significant drop in wave amplitude, especially in the infrared area because these compounds have a highly metallic behavior and the incident light wavelength is greatly reduced and finally absorbed. In Fig. 11(d), along the zz axis, the extinction coefficient at zero energy is very low, but it has a Dirac peak at the visible edge. By increasing the incident photon energy, they all decline (at both directions) with a steep slope to reach zero at high energies. Besides, according to the refractive index value less than one at high energies (after 10 eV) and as it is obvious from Fig. 11(e) and 11(f), the reflection coefficient is also less than 0.2 after 10 eV. Furthermore, considering very small amounts of the real and imaginary parts of the dielectric function, these compounds are transparent and most of the incident light passes through.

4. Conclusion

In this paper, the electron, magnetic, and optical properties of the PtCoBi semiconductor compound [001] films and its bulk state are studied based on the density functional theory employing GGA approximation. The half-metallic behavior of its CoBi-term, CoPt-term and PtBi-term terminations and its block state are investigated. The spin polarization at the Fermi level is -73.2% for the bulk state and for the CoBi-term, PtBi-term and CoPt-term terminations are -64.4% , -64.1% and -40.7% , respectively. Consequently, two CoBi-term and PtBi-term terminations are relatively good candidates for applications in the spintronics industry. In addition, due to their large magnetic moment, they can be used in the giant magneto-resistance (GMR). Owing to the very high static values of the imaginary part of the dielectric function in the xx direction, the metallic behaviors of the terminations are extensively strong while it has decreased in the zz direction. These terminations are good optical transformer for electrons because of their high optical conductivity in the range of 0 to 5 eV. According to the extremely low extinction coefficient, the refractive index is smaller than one and the reflectivity is smaller than 0.2. Moreover, because of very small amounts of the real and imaginary parts of the dielectric function for incident photons with energies greater than 10 eV, these compounds exhibit a transparent behavior.

- [1] R.A. De Groot, F.M. Mueller, P.G. Van Engen, K.H.J. Buschow, *Phys. Rev. Lett.* **50** (25), 2024-2027 (1983).
- [2] F. Lei, C. Tang, S. Wang, W. He, *J. Alloys Compd.* **509** (17), 5187-5189 (2011).
- [3] H. Mori, Y. Odahara, D. Shigyo, T. Yoshitake, E. Miyoshi, *Thin Solid Films.* **520** (15), 4979-4983 (2012).
- [4] R. Guo, G. Liu, X. Wang, H. Rozale, L. Wang, R. Khenata, Z. Wu, *RSC Adv.* **6** (111), 109394-109400 (2016).
- [5] J. Ma, V.I. Hegde, K. Munira, Y. Xie, S. Keshavarz, D.T. Mildebrath, C. Wolverton, A.W. Ghosh, W.H. Butler, *Phys. Rev. B.* **95** (2), 024411 (2017).
- [6] Ștefan Țălu, *Micro and nanoscale characterization of three dimensional surfaces. Basics and applications*, Cluj-Napoca, Romania, Napoca Star Publishing house, 2015.
- [7] A. Boochani, M. Jamal, M. Shahrokhi, B. Nowrozi, M.B. Gholivand, J. Khodadadi, E. Sartipi, M. Amiri, M. Asshabi, A. Yari, *J. Mater. Chem. C* **7**, 13559-13572 (2019).
- [8] T. Gruhn, *Phys. Rev. B.* **82** (12), 125210 (2010).
- [9] D. Kieven, R. Klenk, S. Naghavi, C. Felser, T. Gruhn, *Phys. Rev. B.* **81** (7), 075208 (2010).
- [10] M. Ameri, A. Touia, R. Khenata, Y. Al-Douri, H. Baltache, *Optik.* **124** (7), 570-574 (2013).
- [11] S. Kacimi, H. Mehnane, A. Zaoui, *J. Alloys Compd.* **587**, 451-458 (2014).
- [12] A. Missoum, T. Seddik, G. Murtaza, R. Khenata, A. Bouhemadou, Y. Al-Douri, A. Abdiche, H. Meradji, H. Baltache, *Can. J. Phys.* **92** (10), 1105-1112 (2014).
- [13] S.H. Shah, S.H. Khan, A. Laref, G. Murtaza, *J. Solid State Chem.* **258**, 800-808 (2018).
- [14] M. Naseri, D.M. Hoat, *J. Mol. Graph. Model.* **92**, 249-255 (2019).
- [15] B. Mortazavi, M. Shahrokhi, M. Makaremi, T. Rabczuk, *Appl. Mater. Today* **9**, 292-299 (2017).
- [16] B. Mortazavi, M. Shahrokhi, M. Makaremi, T. Rabczuk, *Nanotechnology* **28**, 115705 (2017).
- [17] B. Mortazavi, G.R. Berdiyrov, M. Shahrokhi, T. Rabczuk, *J. Alloys Compd.* **739**, 643-652 (2018).
- [18] M. Shahrokhi, S. Naderi, A. Fathalian, *Solid State Commun.* **152**, 1012-1017 (2012).
- [19] M. Shahrokhi, *Comput. Mater. Sci.* **156**, 56-66 (2019).
- [20] R. Umamaheswari, M. Yogeswari, G. Kalpana, *J. Magn. Magn. Mater.* **350**, 167-173 (2014).
- [21] M. Rostami, M. Afshari, M. Moradi, *J. Alloys Compd.* **575**, 301-308 (2013).
- [22] M. Allaf Behbahani, M. Moradi, M. Rostami, S. Davatolhagh, *J. Phys. Chem. Solids.* **92**, 85-93 (2016).
- [23] V. Alijani, S. Ouardi, G.H. Fecher, J. Winterlik, S.S. Naghavi, X. Kozina, G. Stryganyuk, C. Felser, E. Ikenaga, Y. Yamashita, S. Ueda, K. Kobayashi, *Phys. Rev. B.* **84** (22), 224416 (2011).
- [24] C. Felser, L. Wollmann, S. Chadov, G.H. Fecher, S.S.P. Parkin, *APL Mater.* **3** (4), 041518-041525 (2015).
- [25] M. Ahmad, Naemullah, G. Murtaza, R. Khenata, S. Bin Omran, A. Bouhemadou, *J. Magn. Magn. Mater.* **377**, 204-210 (2015).

- [26] Y. Jin, P. Kharel, P. Lukashev, S. Valloppilly, B. Staten, J. Her-
ran, I. Tutić, M. Mitrakumar, B. Bhusal, A. O'Connell, K. Yang,
Y. Huh, R. Skomski, *J. Appl. Phys.* **120** (5), 053903 (2016).
- [27] X. Wang, Z. Cheng, H. Yuan, R. Khenata, *J. Mater. Chem. C* **5**
(44), 11559-11564 (2017).
- [28] K. Manna, Y. Sun, L. Muechler, J. Kübler, C. Felser, *Nat. Rev.*
Mater. **3**, 244-256 (2018).
- [29] W. Huang, X. Wang, X. Chen, W. Lu, L. Damewood, C.Y. Fong,
J. Magn. Magn. Mater. **377**, 252-258 (2015).
- [30] A. Boochani, B. Nowrozi, J. Khodadadi, S. Solaymani, S. Jalali-
Asadabadi, *J. Phys. Chem. C* **121** (7), 3978-3986 (2017).
- [31] R. Paudel, F. Zhou, M. Liao, J. Zhu, *J. Phys. Chem. Solids* **136**,
109190 (2020).
- [32] Y. Yang, Z.Y. Feng, J.M. Zhang, *J. Phys. Chem. Solids* **131**,
164-172 (2019).
- [33] M.K. Hussain, K.I. Inad, *Thin Solid Films* **663**, 100-104 (2018).
- [34] Y. Yang, Z.Y. Feng, J.M. Zhang, *Appl. Surf. Sci.* **457**, 403-410
(2018).
- [35] Y. Li, G.D. Liu, X.T. Wang, E.K. Liu, X.K. Xi, W.H. Wang,
G.H. Wu, X.F. Dai, *RSC Adv.* **7** (50), 31707-31713 (2017).
- [36] P. Blaha, K. Schwarz, P. Sorantin, S.B. Trickey, *Comput. Phys.*
Commun. **59** (2), 399-415 (1990).
- [37] K. Schwarz, P. Blaha, *Computational Materials Science* **28** (2),
259-273 (2003).
- [38] C. Ambrosch-Draxl, J.O. Sofo, *Comput. Phys. Commun.* **175** (1),
1-14 (2006).
- [39] R.L. Kronig, *J. Opt. Soc. Am.* **12** (6), 547-557 (1926).
- [40] A. Zheng, H. Huang, G. Gao, K. Yao, *J. Mater. Sci.* **53**, 8364-8371
(2018).
- [41] B. Hamad, *J. Appl. Phys.* **115**, 0-6 (2014).
- [42] N. Nik-Akhtar, A. Vaez, *Phys. E Low-Dimensional Syst. Nano-*
structures **103**, 164-170 (2018).
- [43] W. Khan, G. Murtaza, T. Ouahrani, A. Mahmood, R. Khenata,
M. El Amine Monir, H. Baltache, *J. Alloys Compd.* **674**, 109-115
(2016).
- [44] M. Fox, *Optical Properties of Solids*, 2010 Oxford, New York.